Thermal hysteretic behavior and negative magnetoresistance in the charge density wave material EuTe$_4$

Q. Q. Zhang [1,2,*], Y. Shi [3,*], K. Y. Zhai [1,2], W. X. Zhao [1,2], X. Du [1,2], J. S. Zhou [1,2], X. Gu [1,2]
R. Z. Xu [1,2], Y. D. Li [1,2], Y. F. Guo [4,5], Z. K. Liu [4,5], C. Chen [4,5,6], S.-K. Mo [6], T. K. Kim [7], C. Cacho [7]
J. W. Yu [1,2], W. Li [1,2], Y. L. Chen [4,5,8] Jiun-Haw Chu [3,*] and L. X. Yang [1,2,†]

[1]*State Key Laboratory of Low Dimensional Quantum Physics, Department of Physics, Tsinghua University, Beijing 100084, China*
[2]*Frontier Science Center for Quantum Information, Beijing 100084, China*
[3]*Department of Physics, University of Washington, Seattle, Washington 98195, USA*
[4]*School of Physical Science and Technology, ShanghaiTech University and CAS-Shanghai Science Research Center, Shanghai 201210, China*
[5]*ShanghaiTech Laboratory for Topological Physics, Shanghai 200031, China*
[6]*Advanced Light Source, Lawrence Berkeley National Laboratory, Berkeley, California 94720, USA*
[7]*Diamond Light Source, Didcot OX11 0DE, United Kingdom*
[8]*Department of Physics, Clarendon Laboratory, University of Oxford, Parks Road, Oxford OX1 3PU, United Kingdom*

EuTe$_4$ is a van der Waals material exhibiting a charge density wave (CDW) with a large thermal hysteresis in the resistivity and CDW gap. In this paper, we systematically study the electronic structure and transport properties of EuTe$_4$ using high-resolution angle-resolved photoemission spectroscopy (ARPES), magnetoresistance (MR) measurements, and scanning tunneling microscopy (STM). We observe a CDW gap of $\sim$200 meV at low temperatures that persists up to 400 K, suggesting that the CDW transition occurs at a much higher temperature. The ARPES intensity near the Fermi level shows large thermal hysteretic behavior, consistent with the resistivity measurement. The hysteresis in the resistivity measurement does not change under a magnetic field up to 7 T, excluding the thermal magnetic hysteretic effect. Instead, the surface topography measured with STM shows surface domains with different CDW trimerization directions, which may be important for the thermal hysteretic behavior. Interestingly, we reveal a large negative MR at low temperatures that can be associated with the canting of magnetically ordered Eu spins. Our results shed light on the understanding of magnetic, transport, and electronic properties of EuTe$_4$.

I. INTRODUCTION

In solid materials, the interaction and cooperation between electrons and lattice can induce a long-range ordered ground state in which charge and lattice pattern in a new periodic structure that is different from the normal-state lattice structure [1,2]. Such a charge density wave (CDW) state, since its discovery, has been extensively studied for decades [3–6]. While the consequence of symmetry breaking is evident, the mechanism of the CDW transition in each materials system varies and is often under debate. In a half-filled one-dimensional (1D) electronic system, the nuclear atoms are susceptible to the dimerization due to the perfectly nested Fermi surface (FS), which is accompanied by the fully opened energy gap in the electronic density of states and the softening of the phonons with the momentum of twice the Fermi momentum of the electronic energy band [1]. However, the FS nesting scenario has been challenged [7–10], particularly in many two-dimensional (2D) and three-dimensional (3D) materials [11–14], where the FS is usually not perfectly nested,

resulting in partial energy gaps and metallic CDW states [15–18].

The binary rare-earth polytellurides RTe$_n$ (where R is a rare-earth element, $n = 2$, 2.5, 3, and 4) provide an ideal platform to study CDW transition in van der Waals materials [15–24]. The common structure of these compounds consists of corrugated R-Te slabs and planar square Te sheets that alternately stack along the c axis. The planar square Te nets are highly unstable toward lattice distortion, resulting in commensurate or incommensurate CDW states [25–27]. The $5p$ orbitals of Te atoms in the planar Te nets are partially filled, constructing the electronic energy bands near the Fermi level (E_{F}). The R-derived states, on the other hand, usually locate below E_{F} and make negligible contribution to the FS and CDW order. In general, the CDW transition in RTe$_n$ is interpreted by FS nesting, although most of them remain metallic in the CDW state owing to the imperfect FS nesting [15–17,28].

Recently, rare-earth tetratelluride EuTe$_4$ was discovered to exhibit a nonmetallic CDW state. It crystallizes into an orthorhombic lattice structure with the space group of $Pmmn$ (No. 59) at room temperature. The lattice structure of EuTe$_4$ consists of corrugated Eu-Te layers separated by Te monolayers or bilayers, as schematically shown in Fig. 1(a) [21]. The quasisquare Te nets in EuTe$_4$ are unstable and prone
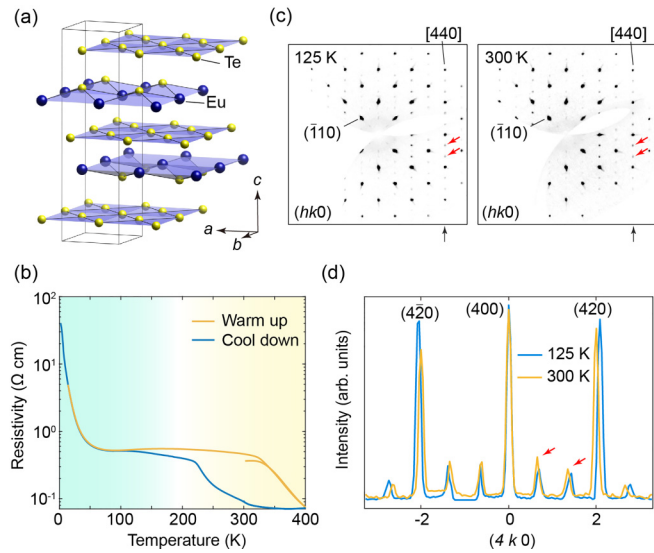
*[*]jhchu@uw.edu
*[†]lxyang@tsinghua.edu.cn

FIG. 1. Basic characterization of EuTe$_4$ single crystal. (a) Illustration of the crystal structure of EuTe$_4$. (b) The temperature dependence of in-plane electrical resistivity. A thermal hysteresis loop is observed in a large temperature range. (c) X-ray diffraction (XRD) pattern along $(hk0)$ at 125 and 300 K, respectively. (d) Line profile of the XRD pattern along the $[4k0]$ direction as indicated by the arrows in (c). The red arrows in (c) and (d) indicate the charge density wave (CDW) superstructure spots and peaks.

to distort, leading to the trimerization of Te atoms. The CDW superstructure was initially determined to be $1a \times 3b \times 2c$ [21]. However, a recent x-ray diffraction (XRD) experiment suggested an incommensurate CDW wave vector of $q_b = 0.643(3)b^*$, where $b^* = 2\pi/b$ [22]. The CDW transition temperature of EuTe$_4$ is still a mystery: while it was initially determined to be $\sim$255 K from the resistivity measurement [21], recent angle-resolved photoemission spectroscopy (ARPES) and XRD measurements suggest that the CDW transition occurs at a much higher temperature >400 K [22,23]. Density functional theory calculation suggests that the CDW transition is driven by FS nesting [29], despite that the crystal structure >400 K remains unknown up to date. Interestingly, both the resistivity and ARPES measured CDW gap show a thermal hysteretic behavior in a large temperature range from 100 to 400 K, which was attributed to the switching of the relative CDW phases in different Te layers [22]. However, compelling evidence of this phenomenological scenario is still lacking, and the thermal hysteretic behavior is still not fully understood.

In this paper, we systematically study the electronic structure and electrical transport property of EuTe$_4$ using high-resolution ARPES, scanning tunneling microscopy (STM), and magnetoresistance (MR) measurement. XRD studies show no obvious change in the lattice structure in the temperature range from 125 to 300 K except for a considerable thermal expansion. The ARPES intensity near E_F shows a considerable thermal hysteresis, in good agreement with the resistivity measurement. The measurement of the resistivity under different magnetic fields excludes the thermal magnetic hysteretic behavior, while the sample surface topography unravels the coexistence of different domains of

oppositely trimerized Te atoms in the same Te layer, which may play an important role in the thermal hysteretic behavior. Interestingly, we observe a negative MR (NMR) of $\sim$86% under a magnetic field > 4 T at 2 K, which is consistent with the realignment of Eu ordered moments. Our results provide insights into the understanding of the properties of EuTe$_4$.

II. METHOD

Single crystals of EuTe$_4$ were synthesized via a Te flux method [21]. Electrical transport measurements were carried out in a Quantum Design physical property measurement system. Electrical contacts were prepared by attaching four Pt wires with silver paste onto evaporated gold pads on the crystal surface. A 1 mA current was applied in the ab plane, and the magnetic field was applied along the c axis.

ARPES measurements were performed at beamline I05 of Diamond Light Source (DLS) [30], beamline 10.0.1 of the Advanced Light Source (ALS), beamline BL13U of National Synchrotron Radiation Laboratory (NSRL), and the laser-based ARPES system in Tsinghua University. Data were collected by Scienta R4000 (DA30 L) analyzers at DLS and ALS (NSRL and Tsinghua University), respectively. Energy and angular resolutions were set to 15 meV (7 meV) and 0.2 ° for synchrotron (laser)-based experiments, respectively. The samples were cleaved *in situ* and measured under ultrahigh vacuum < 1×10^{-10} Torr.

III. RESULTS AND DISCUSSION

Figure 1(b) shows the temperature-dependent resistivity measurement of our sample. The resistivity shows a nonmetallic temperature dependence. We notice that low-temperature resistivity is considerably lower than the value in the previous report [21] and can vary significantly depending on the growth conditions, which is typical for a nearly intrinsic semiconductor. Consistent with previous results, a hysteresis loop is observed in a large temperature range from $\sim$100 to 400 K [21]. Figures 1(c) and 1(d) show XRD patterns at 125 and 300 K in the $(hk0)$ plane, respectively. The superlattice spots exist at both 125 and 300 K, implying a CDW state up to 300 K, consistent with previous results [22]. Therefore, the observed hysteretic behavior is not related to the CDW transition. We estimate a CDW wave vector of $\sim$0.325b^* without noticeable change between 125 and 300 K, which suggests an incommensurate CDW state. The observed shift of the scattering peaks suggests a large linear thermal expansion coefficient of about 2.24×10^{-4}/K.

Figure 2 shows the basic electronic structure of EuTe$_4$. Figures 2(a) and 2(b) depict the 3D plot of ARPES spectra and constant energy contours (CECs) at selected binding energies, respectively. Due to the formation of CDW, the entire FS is gapped, inducing a semiconducting band structure that accords with the resistivity measurement [Fig. 1(b)]. The CECs shown in Fig. 2(b) exhibit zigzag chains that can be well described by the tight-binding model [yellow and cyan curves in Fig. 2(b)], which is like the situation in RTe$_3$ [15–17] and suggests the relevance of FS nesting in the CDW transition [31]. With increasing binding energy, the CEC splits into parallel sheets. We observe weak states that can be connected
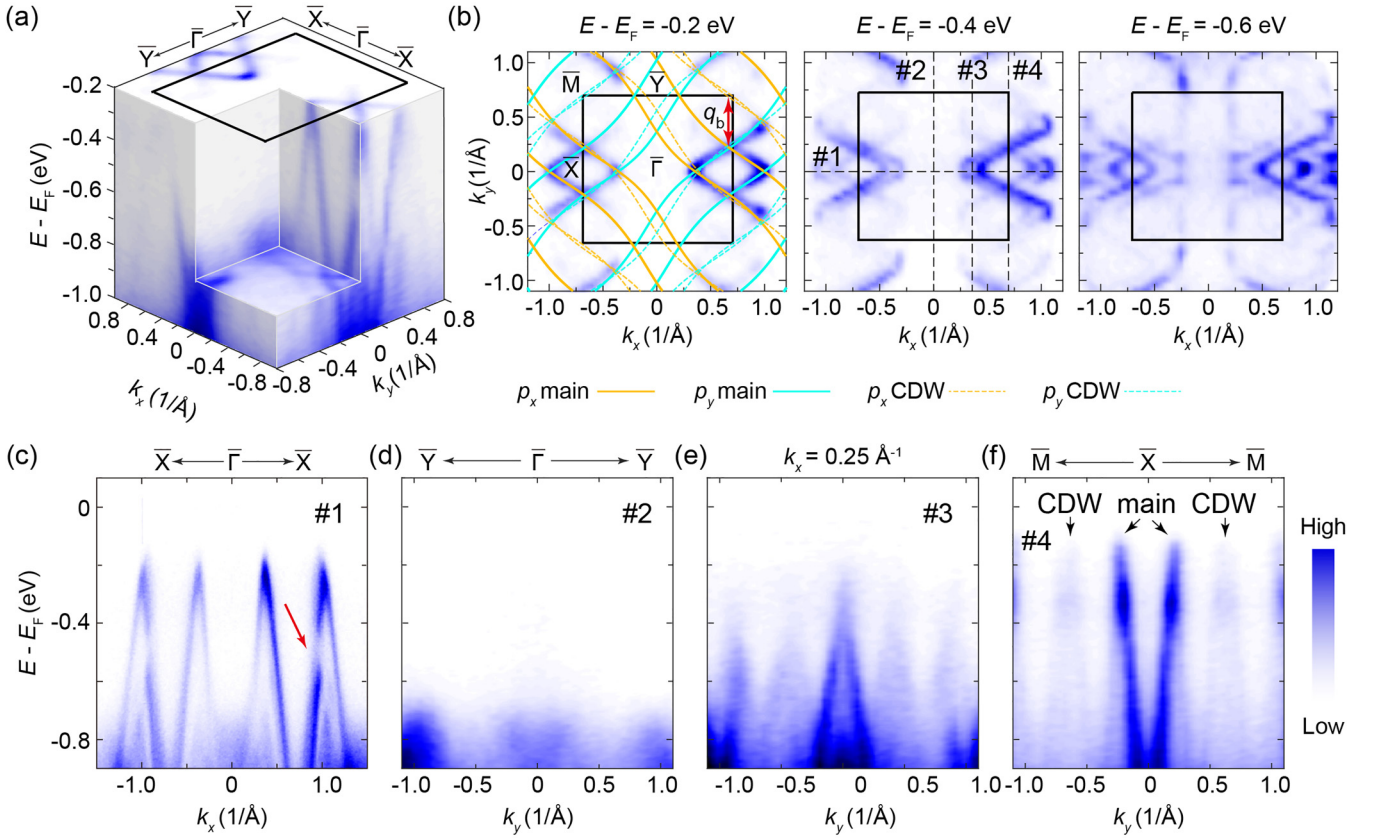
FIG. 2. Basic electronic structure of EuTe$_4$. (a) Three-dimensional plot of the electronic structure of EuTe$_4$. The black lines indicate the surface Brillouin zone (BZ). (b) Constant energy contours (CECs) in the k_x-k_y plane at selected binding energies, which were obtained by integrating angle-resolved photoemission spectroscopy (ARPES) intensity in an energy window of 100 meV. The solid black rectangle represents the surface BZ. The solid cyan and yellow lines are calculated band dispersions by tight-binding model, while the dashed cyan and yellow lines indicate the charge density wave (CDW) folded bands. (c)–(f) The band dispersion along cuts #1–#4 as indicated by the dashed lines in (b). The red arrow in (c) indicates the band modulation near -0.5 eV. The main band and folded band are indicated by the black arrows in (f). Data were collected at 12 K with photon energy $h\nu = 130$ eV.

to the main states by the CDW wave vector [red arrow in Fig. 2(b)], which are identified as CDW-folded states.

Figures 2(c)–2(f) show the band dispersions along high-symmetry directions collected with photon energy $h\nu = 130$ eV at 12 K. Along $\bar{X}\bar{\Gamma}\bar{X}$ (cut #1), we observe linearlike band dispersions in a large energy range with band top at about -200 meV due to the formation of the CDW gap. By contrast, there exists no band dispersions along $\bar{Y}\bar{\Gamma}\bar{Y}$ (cut #2) down to -0.6 eV, suggesting a large anisotropy of the band structure. Along cuts #3 and #4, we observe similar linearlike band dispersions with a CDW gap slightly smaller along $\bar{M}\bar{X}\bar{M}$. The CDW-folded bands are indicated by black arrows in Fig. 2(f), which show much weaker intensity than the main bands. Our experiment agrees with the previous results [22,23], despite the different photon energy used in this paper. We note a band modulation near -0.5 eV, as indicated by the red arrow in Fig. 2(c). This gaplike feature does not show a temperature dependence and exists only in the second Brillouin zone. It may be due to the existence of extra bands with band tops at about -0.7 and -0.55 eV (Supplemental Material, Fig. S1 [32]).

Figure 3 investigates the temperature evolution of the band structure using laser-ARPES. Figure 3(a) shows the electronic structure along the high-symmetry $\bar{\Gamma}\bar{X}$ direction (cut #1) at

selected temperatures. The band structure remains gapped up to 380 K, suggesting a much higher CDW transition temperature. Figure 3(b) shows the energy distribution curves (EDCs) integrated in a momentum window of ~ 0.08 Å^{-1} around the momentum position of the valence band top, from which we observe the change of the peak position and width with temperature. Figure 3(c) shows the leading-edge gap (LEG) as a function of temperature. We observe a thermal hysteresis loop in the LEG, consistent with the previous ARPES measurement [22]. Nevertheless, the hysteresis loop is not so prominent as that in Ref. [22]. The maximum difference between the LEG in the heating up and cooling down branches is ~ 10 meV compared with a difference of ~ 40 meV in Ref. [22]. We suggest that the quantitative difference from Ref. [22] may be due to the differences in samples. Indeed, our sample shows a lower resistivity at low temperatures and a less prominent hysteresis loop in the resistivity curve. Figure 3(d) shows the temperature evolution of ARPES intensity integrated in an energy window of 80 meV near E_F. We notice that the ARPES intensity near E_F shows a large thermal hysteresis loop with the intensity higher in the cooling branch, suggesting that the incoherent electronic states at E_F is important for the resistivity and the thermal hysteretic behavior.
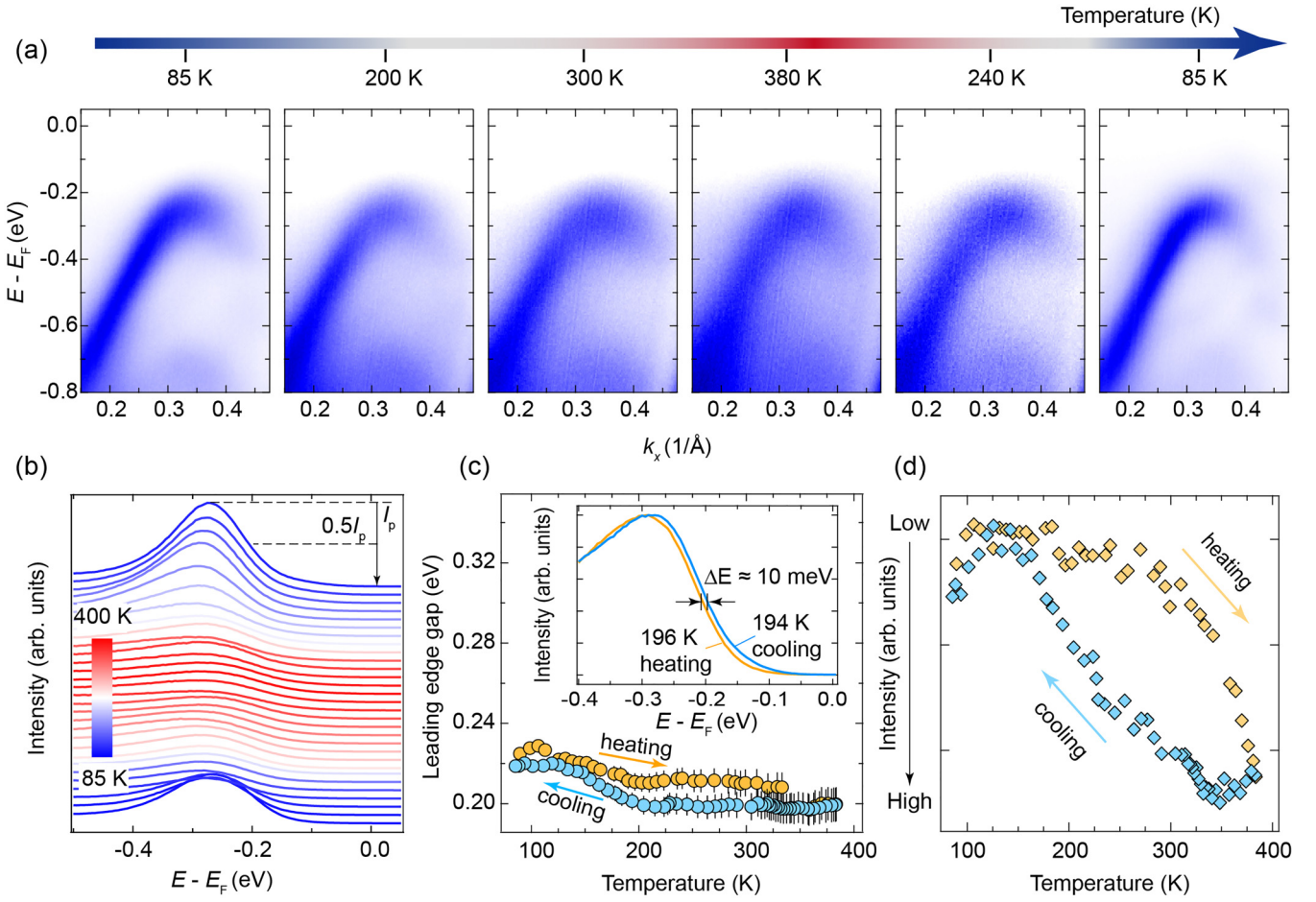
FIG. 3. Temperature evolution of the band structure of EuTe$_4$. (a) Band dispersion along the $\bar{\Gamma}\bar{X}$ direction at selected temperatures. (b) Temperature evolution of the energy distribution curves (EDCs) integrated in a momentum window of about 0.08 Å^{-1} around the momentum position of the band top. (c) Leading edge gap at $0.5I_p$ as a function of temperature, where I_p is the maximum value of the EDC peak as marked in (b). The inset compares two typical EDCs at 196 K during heating up and 194 K during cooling down the sample. (d) Angle-resolved photoemission spectroscopy (ARPES) intensity integrated in an energy window of 80 meV near E_F as a function of temperature. Data were taken with 6.994 eV laser.

The thermal hysteretic phenomena are often observed in CDW materials featuring metastable states during the transition [33–37] and have been interpreted by different mechanisms such as the pinning of the CDW phase to impurities [34], metal-to-insulator transition [33], and incommensurate-to-commensurate CDW transition [37]. In EuTe$_4$, the hysteretic behavior was attributed to the switching of the relative phase of CDWs in different Te layers [22]. However, compelling evidence of such a phenomenological scenario is still lacking.

Figure 4(a) schematically shows the crystal structures of RTe$_n$ compounds. They share the common structure units of R-Te slabs and nearly square Te nets that are energetically unstable to form the periodic distortion of Te atoms [21,25,26]. Among them, RTe$_2$ and RTe$_3$ feature only Te monolayers and bilayers, respectively, while EuTe$_4$ consists of both monolayers and bilayers of Te atoms. The coexistence of electrically neutral Te monolayers and bilayers in EuTe$_4$ was suggested to be crucial for the observed hysteretic behavior [22]. It is noticeable that no hysteretic behavior is observed in R_2Te$_5$, although it also features both Te monolayers and bilayers, which is possibly because the Te layers in R_2Te$_5$ are not

electrically neutral [38]. In addition, EuTe$_4$ consists of unique Eu-Te slabs separated by Te monolayers, which may strongly affect the CDW structure and the hysteretic behavior.

On the other hand, the multi-f-electron nature and the magnetization of Eu atoms may also play a role in the hysteretic behavior. While the change of Eu valence has been ruled out by x-ray absorption near-edge spectroscopy experiments [22], the impact of the magnetization has not been investigated. In Fig. 4(b), we show the resistivity measurements under magnetic fields along the c axis. We observe minor change of the hysteresis loop from 0 to 7 T, which excludes the magnetization as the major mechanism of the hysteretic behavior [39,40].

Moreover, we also checked the CDW structure of the sample by using STM at 4 K. The STM topography in Fig. 4(c) visualizes the trimerization of Te atoms forming chainlike structures [21]. Noticeably, we observe CDW domains with opposite trimerizing directions as indicated by the green and orange rectangles in Fig. 4(c), suggesting the coexistence of out-of-phase CDWs in a single Te layer. Since the opposite trimerizations are energetically degenerate, they can coexist in both Te monolayers and bilayers, thus affecting the 3D
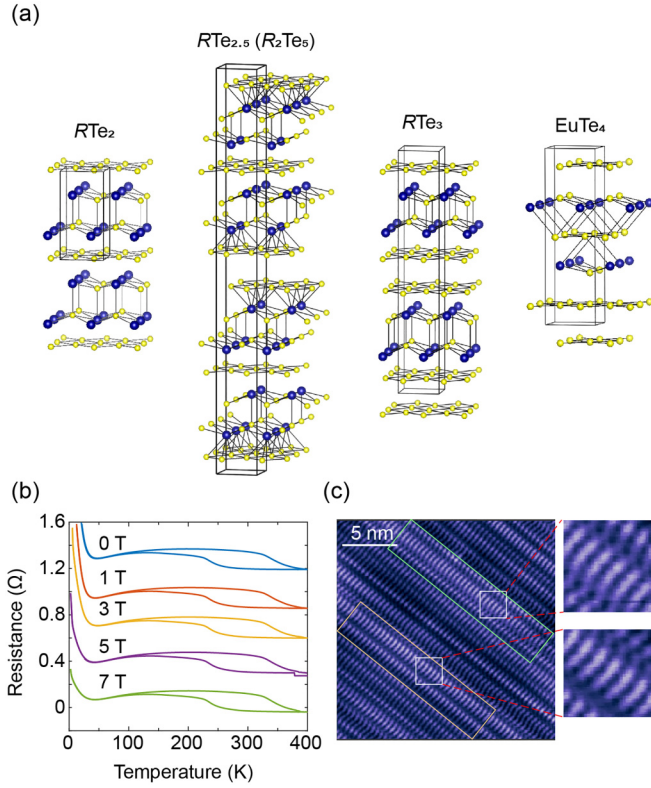
FIG. 4. Possible mechanisms of the thermal hysteretic behavior in EuTe$_4$. (a) The crystal structure of RTe$_n$ compounds, where R is a rare-earth element. (b) Temperature-dependent resistance of EuTe$_4$ under different magnetic fields. (c) Scanning tunneling microscopy (STM) surface topography of the top Te layer. The green and orange rectangles indicate the charge density wave (CDW) domains with opposite trimerizing directions. The insets are the zoom-in plot of the data in the white squares.
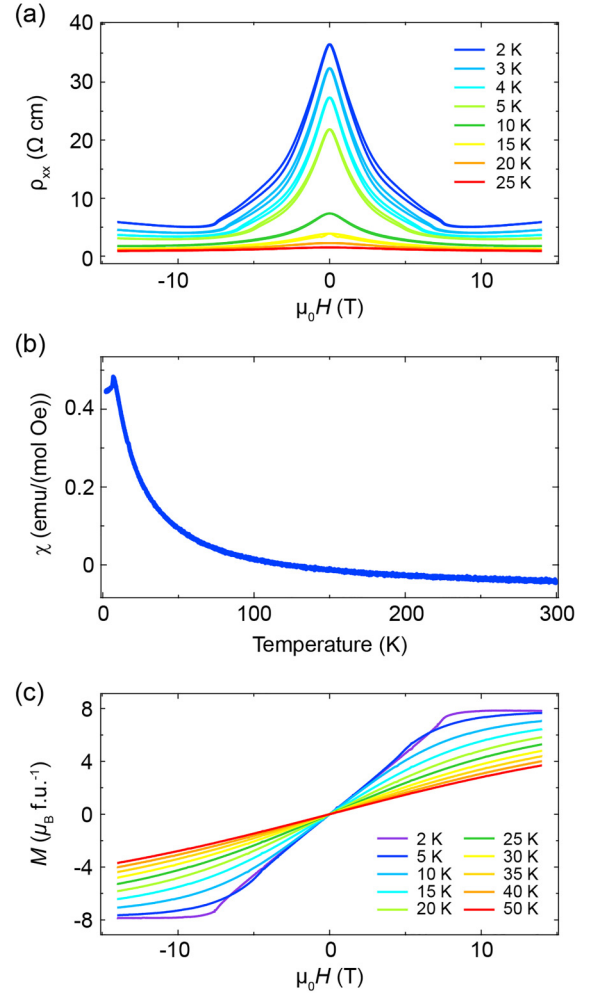

FIG. 5. Magnetoresistance of EuTe$_4$. (a) Magnetoresistivity measured at different temperatures from 2 to 25 K. (b) Magnetic susceptibility as a function of temperature. (c) Magnetization as a function of magnetic field measured at different temperatures.

stacking of the CDWs. We suggest that, like the picture of magnetic domains and magnetic hysteresis loops, the competition of the CDW domains at different temperatures may play an important role in the thermal hysteretic behavior of EuTe$_4$.

Interestingly, in our MR measurement, we observe a decrease of resistivity with increasing magnetic field, as shown in Fig. 5(a). At 2 K, the in-plane resistivity decreases by ∼86%, which is a considerable NMR even larger than the value observed in Fe/Cr/Fe heterostructure (60%) [41]. The NMR effect is suppressed by increasing temperature and finally disappears at 25 K. Figures 5(b) and 5(c) show the magnetic susceptibility and magnetization measurement, respectively. The peak in the temperature dependence of magnetic susceptibility indicates that EuTe$_4$ orders antiferromagnetically <7 K. From the magnetization vs field data, the NMR effect is highly correlated with the canting of the Eu moment toward the c axis. Therefore, the NMR effect is very likely a result of the change of electronic structure due to the realignment of the spins of Eu^{2+} ions. We notice that a similar NMR effect has been observed in a related antiferromagnet EuTe$_2$, which was attributed to a similar spin-flip transition [42]. Magnetic-ordering-related large NMR was also observed in ferromagnetic Eu-based compounds EuIn$_2$P$_2$ and EuIn$_2$As$_2$ near their Curie temperatures [43,44].

IV. CONCLUSIONS

In conclusion, we present a comprehensive investigation on the electronic structure and MR of the van der Waals material EuTe$_4$. We observe a large thermal hysteresis in the resistivity and ARPES intensity near E_F. Several different mechanisms of the thermal hysteretic behavior are discussed. We suggest that the coexistence of opposite trimerization of Te atoms may play an important role in the thermal hysteretic behavior. Moreover, we reveal a large NMR effect in EuTe$_4$ at low temperatures, which may be due to the realignment of the spins of Eu^{2+} ions. The semiconducting nature, thermal hysteretic behavior, and the large NMR effect make EuTe$_4$ an interesting platform for investigating unusual CDW transition in van der Waals materials.

ACKNOWLEDGMENTS

[1] G. Grüner, Rev. Mod. Phys. **60**, 1129 (1988).

[2] G. Gruner and A. Zettl, Phys. Rep. **119**, 117 (1985).

[3] K. Rossnagel, J. Phys.: Condens. Matter **23**, 213001 (2011).

[4] X. Zhu, Y. Cao, J. Zhang, E. W. Plummer, and J. Guo, Proc. Natl. Acad. Sci. USA **112**, 2367 (2015).

[5] C. W. Chen, J. Choe, and E. Morosan, Pep. Prog. Phys. **79**, 084505 (2016).

[6] S. Hellmann, T. Rohwer, M. Kalläne, K. Hanff, C. Sohrt, A. Stange, A. Carr, M. M. Murnane, H. C. Kapteyn, L. Kipp *et al.*, Nat. Commun. **3**, 1069 (2012).

[7] J. Schäfer, M. Sing, R. Claessen, E. Rotenberg, X. J. Zhou, R. E. Thorne, and S. D. Kevan, Phys. Rev. Lett. **91**, 066401 (2003).

[8] L. Perfetti, H. Berger, A. Reginelli, L. Degiorgi, H. Höchst, J. Voit, G. Margaritondo, and M. Grioni, Phys. Rev. Lett. **87**, 216404 (2001).

[9] L. Perfetti, S. Mitrovic, G. Margaritondo, M. Grioni, L. Forró, L. Degiorgi, and H. Höchst, Phys. Rev. B **66**, 075107 (2002).

[10] L. Kang, X. Du, J. S. Zhou, X. Gu, Y. J. Chen, R. Z. Xu, Q. Q. Zhang, S. C. Sun, Z. X. Yin, Y. W. Li *et al.*, Nat. Commun. **12**, 6183 (2021).

[11] M. D. Johannes, I. I. Mazin, and C. A. Howells, Phys. Rev. B **73**, 205102 (2006).

[12] M. D. Johannes and I. I. Mazin, Phys. Rev. B **77**, 165135 (2008).

[13] D. S. Inosov, V. B. Zabolotnyy, D. V. Evtushinsky, A. A. Kordyuk, B. Büchner, R. Follath, H. Berger, and S. V. Borisenko, New J. Phys. **10**, 125027 (2008).

[14] D. W. Shen, B. P. Xie, J. F. Zhao, L. X. Yang, L. Fang, J. Shi, R. H. He, D. H. Lu, H. H. Wen, and D. L. Feng, Phys. Rev. Lett. **99**, 216404 (2007).

[15] G.-H. Gweon, J. D. Denlinger, J. A. Clack, J. W. Allen, C. G. Olson, E. DiMasi, M. C. Aronson, B. Foran, and S. Lee, Phys. Rev. Lett. **81**, 886 (1998).

[16] V. Brouet, W. L. Yang, X. J. Zhou, Z. Hussain, N. Ru, K. Y. Shin, I. R. Fisher, and Z. X. Shen, Phys. Rev. Lett. **93**, 126405 (2004).

[17] F. Schmitt, P. S. Kirchmann, U. Bovensiepen, R. G. Moore, L. Rettig, M. Krenz, J. H. Chu, N. Ru, L. Perfetti, D. H. Lu *et al.*, Science **321**, 1649 (2008).

[18] V. Brouet, W. L. Yang, X. J. Zhou, Z. Hussain, R. G. Moore, R. He, D. H. Lu, Z. X. Shen, J. Laverock, S. B. Dugdale *et al.*, Phys. Rev. B **77**, 235104 (2008).

[19] D. R. Garcia, G. H. Gweon, S. Y. Zhou, J. Graf, C. M. Jozwiak, M. H. Jung, Y. S. Kwon, and A. Lanzara, Phys. Rev. Lett. **98**, 166403 (2007).

[20] A. Kogar, A. Zong, P. E. Dolgirev, X. Shen, J. Straquadine, Y.-Q. Bie, X. Wang, T. Rohwer, I. C. Tung, Y. Yang *et al.*, Nat. Phys. **16**, 159 (2019).

[21] D. Wu, Q. M. Liu, S. L. Chen, G. Y. Zhong, J. Su, L. Y. Shi, L. Tong, G. Xu, P. Gao, and N. L. Wang, Phys. Rev. Mater. **3**, 024002 (2019).

[22] B. Q. Lv, A. Zong, D. Wu, A. V. Rozhkov, B. V. Fine, S. D. Chen, M. Hashimoto, D. H. Lu, M. Li, Y. B. Huang *et al.*, Phys. Rev. Lett. **128**, 036401 (2022).

[23] C. Zhang, Q.-Y. Wu, Y.-H. Yuan, X. Zhang, H. Liu, Z.-T. Liu, H.-Y. Zhang, J.-J. Song, Y.-Z. Zhao, F.-Y. Wu *et al.*, Phys. Rev. B **106**, L201108 (2022).

[24] K. Y. Shin, J. Laverock, Y. Q. Wu, C. L. Condron, M. F. Toney, S. B. Dugdale, M. J. Kramer, and I. R. Fisher, Phys. Rev. B **77**, 165101 (2008).

[25] C. Malliakas, S. J. Billinge, H. J. Kim, and M. G. Kanatzidis, J. Am. Chem. Soc. **127**, 6510 (2005).

[26] R. Patschke and M. G. Kanatzidis, Phys. Chem. Chem. Phys. **4**, 3266 (2002).

[27] W. Tremel and R. Hoffmann, J. Am. Chem. Soc. **109**, 124 (1987).

[28] R. G. Moore, V. Brouet, R. He, D. H. Lu, N. Ru, J. H. Chu, I. R. Fisher, and Z. X. Shen, Phys. Rev. B **81**, 073102 (2010).

[29] A. Pathak, M. K. Gupta, R. Mittal, and D. Bansal, Phys. Rev. B **105**, 035120 (2022).

[30] M. Hoesch, T. K. Kim, P. Dudin, H. Wang, S. Scott, P. Harris, S. Patel, M. Matthews, D. Hawkins, S. G. Alcock *et al.*, Rev. Sci. Instrum. **88**, 013106 (2017).

[31] J. Laverock, S. B. Dugdale, Z. Major, M. A. Alam, N. Ru, I. R. Fisher, G. Santi, and E. Bruno, Phys. Rev. B **71**, 085114 (2005).

[32] See Supplemental Materials at http://link.aps.org/supplemental/10.1103/PhysRevB.107.115141 for the existence of extra bands.

[33] X. Granados, J. Fontcuberta, X. Obradors, and J. B. Torrance, Phys. Rev. B **46**, 15683 (1992).

[34] C. S. Lue, Y. K. Kuo, F. H. Hsu, H. H. Li, H. D. Yang, P. S. Fodor, and L. E. Wenger, Phys. Rev. B **66**, 033101 (2002).

[35] W. Wang, D. Dietzel, and A. Schirmeisen, Sci. Rep. **9**, 7066 (2019).

[36] Y. D. Wang, W. L. Yao, Z. M. Xin, T. T. Han, Z. G. Wang, L. Chen, C. Cai, Y. Li, and Y. Zhang, Nat. Commun. **11**, 4215 (2020).

[37] K. Hamano, T. Hishinuma, and K. Ema, J. Phys. Soc. Jpn. **50**, 2666 (1981).

[38] C. D. Malliakas, M. Iavarone, J. Fedor, and M. G. Kanatzidis, J. Am. Chem. Soc. **130**, 3310 (2008).

[39] J. Dho, W. S. Kim, and N. H. Hur, Phys. Rev. Lett. **87**, 187201 (2001).

[40] L. Wang, Y. G. Cui, J. F. Wan, J. H. Zhang, and Y. H. Rong, AIP Adv. **3**, 082126 (2013).

[41] M. N. Baibich, J. M. Broto, A. Fert, F. Nguyen Van Dau, F. Petroff, P. Etienne, G. Creuzet, A. Friederich, and J. Chazelas, Phys. Rev. Lett. **61**, 2472 (1988).

[42] J. Y. Yin, C. W. Wu, L. S. Li, J. Yu, H. L. Sun, B. Shen, B. A. Frandsen, D. X. Yao, and M. Wang, Phys. Rev. Mater. **4**, 013405 (2020).

[43] J. Jiang and S. M. Kauzlarich, Chem. Mater. **18**, 435 (2006).

[44] A. M. Goforth, P. Klavins, J. C. Fettinger, and S. M. Kauzlarich, Inorg. Chem. **47**, 11048 (2008).